

Antimonene-based saturable absorber for a soliton mode-locked and *Q*-switched fiber laser in the 2 μm wavelength region

H Ahmad, B Nizamani, M Z Samion, N Yusoff, and M F Ismail

Citation: Chin. Phys. B, 2023, 32 (**6**): 064205. DOI: 10.1088/1674-1056/ac891f
Journal homepage: http://cpb.iphy.ac.cn; http://iopscience.iop.org/cpb

What follows is a list of articles you may be interested in

A 54-fs diode-pumped Kerr-lens mode-locked Yb:$LuYSiO_5$ laser

Yang Yu(于洋), Yuehang Chen(陈月航), Wenlong Tian(田文龙), Li Zheng(郑立), Geyang Wang(王阁阳), Chuan Bai(白川), Xuan Tian(田轩), Haijing Mai(麦海静), Yulong Su(苏玉龙), Jiangfeng Zhu(朱江峰), and Zhiyi Wei(魏志义)

Chin. Phys. B, 2023, 32 (**6**): 064204. DOI: 10.1088/1674-1056/acb9ed

A cladding-pumping based power-scaled noise-like and dissipative soliton pulse fiber laser

Zhiguo Lv(吕志国), Hao Teng(滕浩), and Zhiyi Wei(魏志义)

Chin. Phys. B, 2023, 32 (**2**): 024207. DOI: 10.1088/1674-1056/ac8f3e

Yb:CaF_2–YF_3 transparent ceramics ultrafast laser at dual gain lines

Xiao-Qin Liu(刘晓琴), Qian-Qian Hao(郝倩倩), Jie Liu(刘杰), Dan-Hua Liu(刘丹华), Wei-Wei Li(李威威), and Liang-Bi Su(苏良碧)

Chin. Phys. B, 2022, 31 (**11**): 114205. DOI: 10.1088/1674-1056/ac720f

All-fiber erbium-doped dissipative soliton laser with multimode interference based on saturable-reserve saturable hybrid optical switch

Xin Zhao(赵鑫), Renyan Wan(王仁严), Weiyan Li(李卫岩), Liang Jin(金亮), He Zhang(张贺), Yan Li(李岩), Yingtian Xu(徐英添), Linlin Shi(石琳琳), and Xiaohui Ma(马晓辉)

Chin. Phys. B, 2022, 31 (**6**): 064215. DOI: 10.1088/1674-1056/ac5611

Sequential generation of self-starting diverse operations in all-fiber laser based on thulium-doped fiber saturable absorber

Pei Zhang(张沛), Kaharudin Dimyati, Bilal Nizamani, Mustafa M. Najm, and S. W. Harun

Chin. Phys. B, 2022, 31 (**6**): 064204. DOI: 10.1088/1674-1056/ac3ba9

Antimonene-based saturable absorber for a soliton mode-locked and *Q*-switched fiber laser in the 2 μm wavelength region

H Ahmad[1,2,3,†], B Nizamani[1], M Z Samion[1], N Yusoff[1], and M F Ismail[1]

[1] *Photonics Research Centre, Universiti Malaya, 50603 Kuala Lumpur, Malaysia*

[2] *Physics Department, Faculty of Science, Universiti Malaya, 50603 Kuala Lumpur, Malaysia*

[3] *Distinguished Visiting Professor, Universiti Kuala Lumpur British Malaysian Institute (UniKL BMI), Batu 8, Jln Sungai Pusu, 53100, Selangor, Malaysia*

(Received 9 June 2022; revised manuscript received 2 August 2022; accepted manuscript online 12 August 2022)

We demonstrate antimonene as a saturable absorber (SA) to generate an ultrafast mode-locked and *Q*-switched laser in the 2 μm wavelength region. The two antimonene-based SAs were prepared and inserted separately in a thulium–holmium-doped fiber laser to produce the pulsed laser. Antimonene was coated onto a tapered fiber to generate soliton mode-locked pulses and used in thin-film form for the generation of *Q*-switched pulses. The mode-locking was stable within a pump power of 267 mW–511 mW, and the laser operated at a central wavelength of 1897.4 nm. The mode-locked laser had a pulse width of 1.3 ps and a repetition rate of 12.6 MHz, with a signal-to-noise ratio of 64 dB. *Q*-switched laser operation was stable at a wavelength of 1890.1 nm within a pump power of 312 mW–381 mW. With the increase in pump power from 312 mW to 381 mW, the repetition rate increased to a maximum of 56.63 kHz and the pulse width decreased to a minimum value of 2.85 μs. Wide-range tunability of the *Q*-switched laser was also realized within the wavelength range of 1882 nm–1936 nm.

Keywords: mode-locking, *Q*-switched fiber laser, optical saturable absorber

PACS: 42.60.Fc, 42.60.Gd, 42.55.Wd, 42.70.–a **DOI:** 10.1088/1674-1056/ac891f

1. Introduction

Laser technology has gained the attention of researchers due to its extensive applications in military, medical, telecommunications, materials engineering and long-range optical fiber sensing fields.[1–7] All-fiber-based passive lasers can operate at different wavelength regions such as 1 μm, 1.5 μm, and 2 μm depending on the gain medium used. For instance, an ytterbium-doped fiber laser can operate at a wavelength of 1 μm, and 1.5 μm lasing can be achieved by using an erbium-doped fiber laser (EDFL).[8–10] The 1.5 μm laser domain is typically limited to backbone telecommunication network applications only. On the other hand, lasing in a 2 μm wavelength regime can be achieved by a thulium-doped fiber laser (TDFL) or a thulium–holmium-doped fiber laser (THDFL).[11,12] These lasers operate at a wavelength range of around 1.7 μm–2.2 μm, which is an eye-safe region.[13] As there is reasonable water absorption in this region and some gas molecules such as carbon dioxide are present in the environment, there will be strong absorption occurring at 2 μm. Lasers operating in this regime have attracted researchers for their potential use in medical, light detection and ranging (LIDAR) and gas-sensing applications.[14,15] The two techniques commonly used to initiate laser pulsing are mode-locked and *Q*-switched approaches. The strategies for achieving these pulsed lasers use active or passive means. Among them, active techniques usually require external signal modulators to trigger the pulses.[16,17] On the other hand, a saturable absorber (SA) can initiate signal modulation to generate pulses from a continuous-wave (CW) laser without the need for any external active modulator.[18–20] Ultrafast techniques can generate short pulses in the region of nanoseconds (10^{-9} s) to femtoseconds (10^{-15} s). Ultrashort pulses are very important for scientists and can generate new findings such as changes in molecular structure. In materials science, for instance, the physics of matter such as lattice vibration occurs in femtoseconds and atomic diffusion occurs in nanoseconds.[21]

There is an extensive literature on the production of pulsed lasers based on SAs dating from the early work using semiconductor saturable absorber mirrors (SESAMs) by Keller *et al.*[18] The alignment issue and low damage threshold associated with SESAMs led researchers to explore other SA materials. Real SAs are formed by materials that have sufficient nonlinear optical absorption to trigger the laser pulses by passive means. These SAs can be produced by various techniques such as thin film formation using polymer hosts,[22–24] direct dripping over fiber ferrules,[25] drop-casting over side-polished fibers[26] and electron-beam deposition over D-shaped fibers.[27,28] These real SAs have proven to be promising devices for producing ultrashort pulses in all-fiber lasers.

Earlier, carbon nanotubes (CNTs) were reported to produce ultra-fast lasers, demonstrating their shortest pulse width in picoseconds to femtoseconds.[29,30] However, the geometry of CNTs is rather complex, making the bandgap tunability and SA fabrication process complex. Graphene has been extensively reported as an SA in the 1 μm, 1.5 μm and 2 μm

†Corresponding author. E-mail: harith@um.edu.my

© 2023 Chinese Physical Society and IOP Publishing Ltd

wavelength regimes for generating pulsed lasers.[31–33] Since graphene has the limitation of a low damage threshold, a compromise has to be made on operating the laser at lower pump powers to protect the graphene-based SAs.[34] In contrast to graphene, black phosphorus (BP) has broadband optical absorption and a BP SA can produce the shortest pulses of up to 272 fs.[35] Unfortunately, BP is a hydrophilic material that reacts with the oxygen in the atmosphere. This can be favorable for sensing applications but the lasing performance may degrade over time under normal laboratory conditions.[36,37] Since then, two-dimensional materials have gained the attention of researchers for use as SAs because of their nonlinear optical response and suitable optoelectronic properties.[38,39] Recently, the family of MXenes and MAX-phases has been demonstrated to perform well as a SA to achieve ultra-fast fiber lasers.[40–45] A few other material categories have also been explored to produce *Q*-switched and mode-locked lasers, such as transition metal dichalcogenides, metals, transparent conductive oxides and organic materials.[8,46–53]

Furthermore, ternary transition metal dichalcogenides (TTMDs) have also recently gained the interest of researchers for ultrafast photonics. TTMDs involve three-elemental compositions to achieve the optimum electrical and optical response of materials for various applications. These TTMDs were recently integrated into fiber laser cavities to achieve numerous *Q*-switched and mode-locked lasers.[54–56] For instance, $W_xNb_{(1-x)}Se_2$ and $Re_xNb_{(1-x)}S_2$ nanosheets were integrated into EDFLs to achieve *Q*-switched and mode-locked laser pulses at 1.5 μm wavelength. Ultrashort soliton mode-locked pulses of 131 fs and 285 fs were achieved using these TTMDs.[55,56] However, for a three-elemental material composition the physical and chemical limitations of all three elements must always be taken into consideration. Lately, rare-earth oxides such as yttrium oxide (Y_2O_3) have also been used as SAs to initiate mode-locked EDFLs operating at 1.5 μm wavelength.[57] Antimonene, a novel two-dimensional material, has recently gained the attention of researchers for its applications in optoelectronics and fiber lasers and can be formed in nanosheets similar to TTMDs.[56,58–60] The optical absorption of antimonene was studied in the ultraviolet (UV) to infrared (IR) wavelength range, proving that antimonene is a potential candidate for applications such as solar cells and supercapacitors.[61–63] The semiconducting behavior of antimonene is also another interesting feature in regard to its use as a SA.[64,65]

Bulk antimonene behaves like a semimetal with good electrical conductivity and was expected to have similar behavior to a few layers.[66] An indirect bandgap of 2.28 eV was predicted for monolayer antimonene, which was likely to be altered to a direct bandgap under certain physical conditions.[67] This indicates the possibility of a wide variation in the bandgap of antimonene. Antimonene shows a nonlinear absorption behavior similar to other two-dimensional materials such as TTMDs, BP and graphene.[68] When light is incident on antimonene nanosheets, the electrons jump from the ground state to the excited state by gaining energy from the incident photons. After a certain period, the electrons release energy and fall into the middle of the conduction band and valence band. When the incident light is intense enough, the electrons halt the absorption of excess photons (optical bleaching), validating Pauli's blocking principle in which multiple electron states cannot be occupied simultaneously. Wu *et al.* have reported the promising optical nonlinear response of antimonene nanosheets for possible application as a SA for pulsed laser generation.[69] Additionally, antimonene has a fast recovery time of about 2 ps in the visible band spectrum, which allows antimonene to generate ultrashort pulses.[66] The nonlinear optical behavior of antimonene and its significant optical Kerr nonlinearity pave the way for its potential applications as an optical switcher or beam shaper.[70]

Although antimony has been explored as a SA at different wavelength regimes of 1 μm, 1.5 μm and 2 μm,[71–73] antimonene is rarely investigated as a SA for passive generation of *Q*-switched and mode-locked lasers. Currently, antimonene has only been reported as a *Q*-switcher at the C-band wavelength region by integrating it into an EDFL.[74,75] In this work, we report the incorporation of an antimonene-based SA in a THDFL to achieve mode-locked and *Q*-switched pulses at a longer wavelength of 2 μm. The ability of antimonene-based SAs to produce pulsed lasers at this wavelength region is demonstrated for the first time. The achieved mode-locked laser operated at a central wavelength of 1897.4 nm and *Q*-switched pulses were achieved at 1890.1 nm. The *Q*-switched laser was also broadly tunable from 1882 nm to 1936 nm by adding a tunable bandpass filter (TBF) to the laser cavity. The antimonene-based SA could produce both *Q*-switched and mode-locked lasers in the eye-safe region of 2 μm wavelength as a potential laser source for various industrial applications.

2. Preparation and characterization of antimonene-based SAs

The liquid phase exfoliation (LPE) technique was performed to synthesize a few layers of antimonene from its bulk state. One hundred milligrams of antimony powder was first dissolved in 10 ml of isopropyl alcohol solution and stirred for 15 min on a magnetic stirrer under normal conditions to obtain a 10 $mg{\cdot}ml^{-1}$ concentration of antimony suspension. The solution was then sonicated for 8 h in a bath sonicator for the exfoliation process. The antimony was exfoliated in the sonication process, which breaks the weak interlayer bonds in antimony, resulting in a few layers of antimony known as antimonene. To remove the unexfoliated antimony powder, the suspension was centrifuged for 10 min at 4000 rpm. The black

supernatant containing a few layers of antimonene was then collected and stored in a glass vial before being used as a SA.

A Raman spectroscope (Renishaw inVia Raman) equipped with a 532 nm laser was used to obtain the Raman spectrum for both antimony and the antimonene samples, as depicted in Fig. 1. Based on the Raman spectrum of antimony, two Raman peaks can be observed at 117 cm^{-1} and 140 cm^{-1}, which correspond to the E_g and A_{1g} modes, respectively. The in-plane longitudinal vibrational mode of antimony is designated by E_g, whereas the out-of-plane vibrational mode is designated by A_{1g}.[76] These two characteristics of Raman peaks witness a change towards a higher wavenumber, as evidenced in the Raman spectrum of antimonene. The E_g peak shifted from 117 cm^{-1} to 145 cm^{-1} while the A_{1g} peak moved from 140 cm^{-1} to 188 cm^{-1}. It has been reported that the changes in antimony thickness cause the peak position to shift;[77] therefore this shows the successful synthesis of antimonene from bulk antimony.

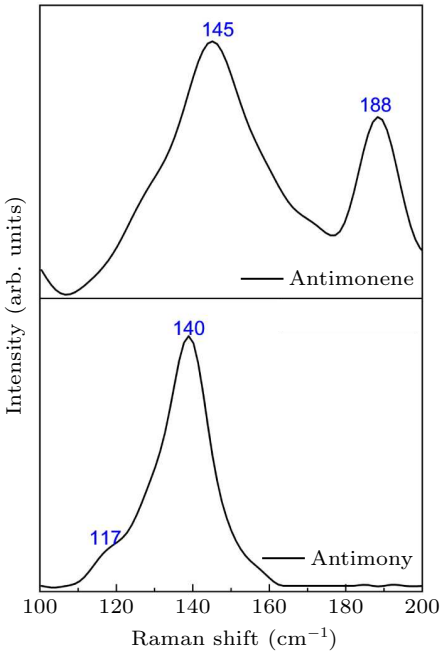


Fig. 1. Raman spectrum of antimony and antimonene.

The morphology of antimonene was investigated using field emission scanning electron microscope [FESEM; JEOL JSM 7600-F FESEM equipped with an energy dispersive x-ray (EDX) detector] at an operating voltage of 2.0 kV and high-resolution transmission electron microscope (HRTEM; JEM 2100-F HRTEM) with an accelerating voltage of 200 kV. Figure 2(a) shows the FESEM image of antimonene which was obtained after the LPE process. The antimonene flakes are seen to have uneven forms and sizes, with the lateral dimension of the flakes ranging from a few hundred nanometers to a few micrometers. Figure 2(b) displays the HRTEM image of antimonene observed at low magnification (15000×); a high-magnification (800000×) HRTEM image of antimonene in the selected area is shown as an inset in Fig. 2(b). The obtained result further proves that the prepared antimonene has a flake-like morphology, and is made up of stacks of a few antimonene layers. Furthermore, the observed bright contrast on the HRTEM image is evidence for the formation of a thin layer of antimonene after the LPE process.

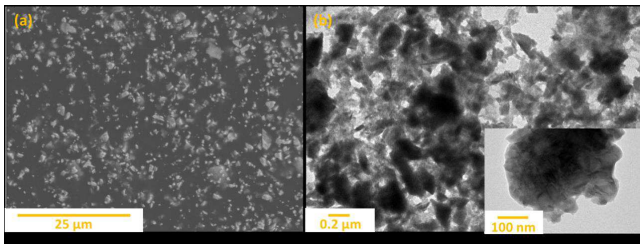


Fig. 2. (a) FESEM and (b) HRTEM images of antimonene (inset: zoomed-in HRTEM image of antimonene).

Figure 3 shows the EDX spectrum and elemental mapping (inset) of antimonene. Based on the EDX spectrum obtained, several energy peaks referring to the elements carbon (C), oxygen (O) and antimony (Sb) can be observed. Carbon and oxygen are common elements present in the environment or surroundings, whereas antimony is the main constituent of antimonene. No signal from other impurity elements can be detected, indicating the high purity of the prepared antimonene.

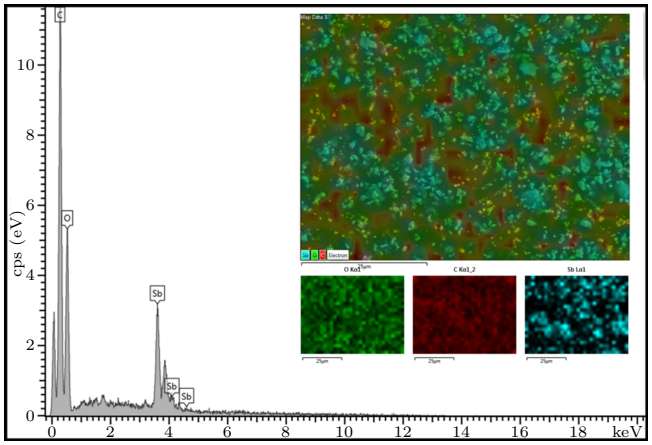


Fig. 3. EDX spectrum of antimonene (inset: EDX elemental mapping of antimonene).

To use antimonene as a mode-locker, the antimonene was deposited onto a tapered fiber and then incorporated in the THDFL. The tapered fiber was first prepared via the flame brushing technique, as explained in our previous work.[78] The insertion loss of the tapered fiber was around 3.2 dB and the fiber waist diameter was reduced to about 9 μm. Then, around 10 μl of antimonene solution was drop cast over the tapered region of the optical fiber and left to dry at room temperature. Figure 4(a) shows a microscope image of the antimonene-coated tapered fiber and figure 4(b) illustrates the drop-casting process of antimonene over the tapered fiber.

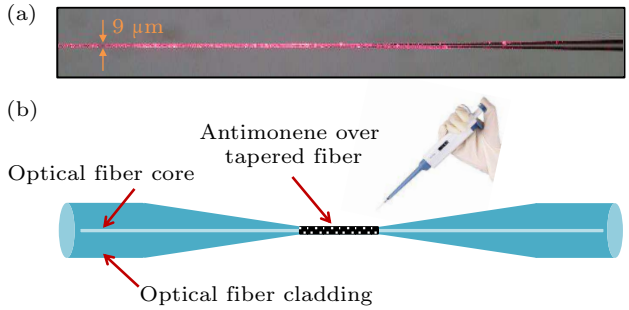


Fig. 4. Antimonene coated over tapered fiber (a) microscopic image, and (b) illustration of antimonene coated tapered fiber.

The evanescent field interaction is achieved by using the tapered fiber in which the light–matter interaction particularly occurs in the tapered region of the optical fiber. Typically, the signal propagates in the fiber core/cladding and a portion of it penetrates the surrounding environment, which is the coated SA material. As such, this evanescent field will interact with the nonlinear optical material, which in this case is antimonene. This technique has the advantage of providing a longer light–matter interaction, avoiding optical damage to the SA, and also having low laser-induced thermal damage.[79,80]

For generation of Q-switched pulses, an antimonene/poly(vinyl alcohol) (PVA) film was fabricated using the solution-casting method. Initially, the PVA solution was prepared by adding 100 mg of PVA powder into a glass beaker containing 10 ml of deionized water. The suspension was then stirred at 60 °C to form a homogeneous solution of PVA with a concentration of 10 mg·ml^{-1}. Next, 10 ml of PVA solution was mixed with 10 ml of antimonene solution and stirred at a temperature of 60 °C until only a third of the original solution was left. Then, the mixture was relocated into a glass Petri dish and dried overnight in an oven at 60 °C. The antimonene/PVA film produced was then peeled off from the Petri dish to be used as a SA. The fiber ferrules were first cleaned using lens cleaning tissue and then a small portion of antimonene thin film was cut and transferred over the fiber ferrule tip, as shown in Figs. 5(a) and 5(b). The antimonene thin film was held over the fiber ferrule using an index-matching gel. The thin film was then sandwiched between two fiber ferrules using a FC/PC fiber connecter as shown in Fig. 5(c). The SA was then integrated into the THDFL to generate Q-switched and tunable Q-switched fiber lasers.

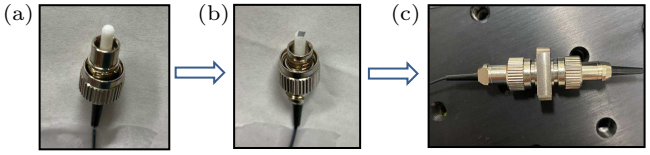


Fig. 5. Antimonene thin-film SA (a) clean fiber ferrule, (b) antimonene thin film over fiber ferrule, and (c) sandwiching of antimonene thin film between fiber ferrules.

The optical characterization of antimonene-based SAs is shown in Fig. 6. Figures 6(a) and 6(b) show the linear absorption of both SAs within the wavelength range 1850 nm–1950 nm. The measurement was done by using an amplified stimulated emission (ASE) source at a low intensity of 0.25 mW output power, together with an optical spectrum analyzer (OSA) at 1 nm resolution. The linear absorption near a wavelength of 1900 nm was around 11 dB for the tapered fiber coated with antimonene and 6.7 dB for the antimonene thin film.

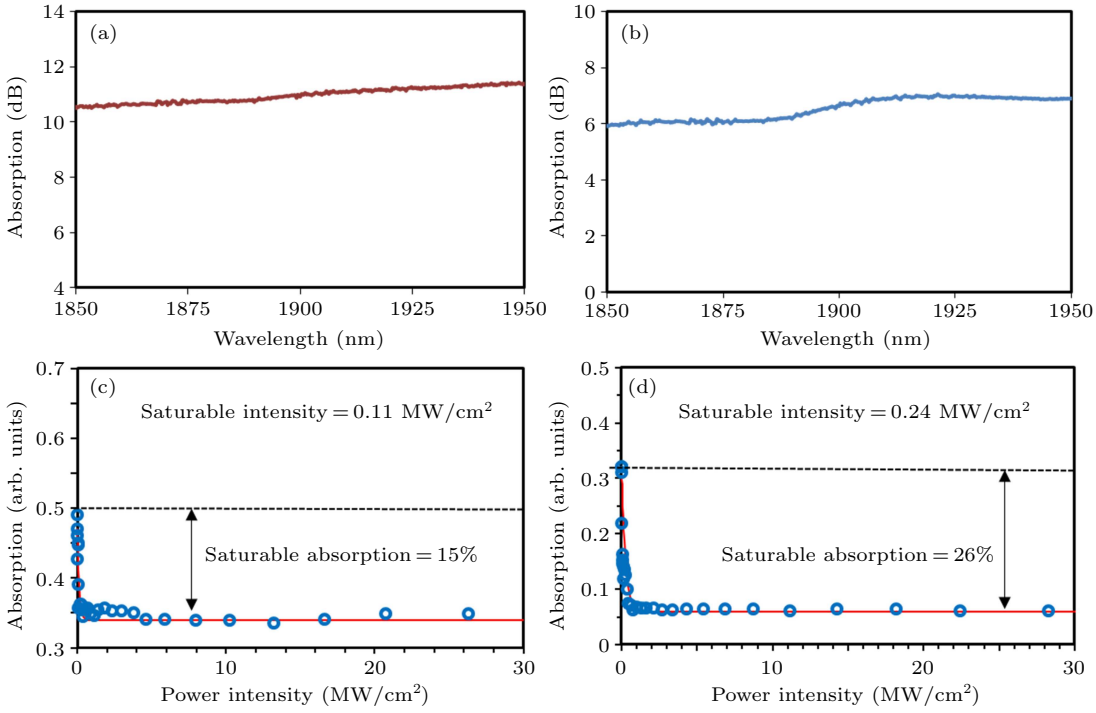


Fig. 6. Optical characterization of antimonene saturable absorbers (a) linear absorption of antimonene coated tapered fiber, (b) linear absorption of antimonene thin film, (c) nonlinear absorption of antimonene coated tapered fiber, and (d) nonlinear absorption of antimonene thin film.

A balanced twin detection measurement was performed to characterize the nonlinear optical response of the two SAs. The characterization for both the SAs was performed separately using the same setup. A mode-locked pulse laser operates at a central wavelength, repetition rate and pulse width of 1950.7 nm, 30 MHz and 4.57 ps, respectively. The amplified output of the pulsed laser was then connected with a variable optical attenuator (VOA) having a maximum attenuation of 50 dB. A 3 dB coupler was connected at the output of VOA to split the signal in a 50:50 ratio. One output end of the 3 dB coupler was then connected to a single-mode fiber (SMF) as a reference and the other end was connected to the SA. Two optical power meters were then connected simultaneously at the output ends to measure the output power from the reference SMF and the SA. The attenuation of the VOA was then tuned from 0 dB to 50 dB and the output power readings were then measured *in situ* at intervals of every 1 dB attenuation. The data were then plotted as illustrated in Figs. 6(c) and 6(d). Figure 6(c) shows the nonlinear absorption of the tapered fiber coated with antimonene and figure 6(d) shows the saturable absorption graph of antimonene thin film. The experimental data (blue circles) was fitted (red line) using Eq. (1), where α_o, α_{ns}, I and I_{sat} are the modulation depth, non-saturable absorption, input intensity and saturation intensity, respectively.[81] For the tapered fiber coated with antimonene, the saturable absorption, non-saturable absorption and saturation intensity were 15%, 34%, and 0.11 MW·cm^{-2}, respectively. For the antimonene thin film, the saturable absorption was 26%, the saturation intensity was 0.24 MW·cm^{-2} and the non-saturable absorption was 6%

$$\alpha(I) = \frac{\alpha_0}{\left(1 + \frac{I}{I_{sat}}\right)} + \alpha_{ns}. \tag{1}$$

3. Experimental setup

Figure 7 shows the experimental setup of the THDFL cavity to generate mode-locked and Q-switched pulse lasers. The gain medium was dual pumped using the two 1560 nm laser diodes (LDs) as the optical power sources. Both the LDs were separately connected with 1550 nm polarization-independent isolators for protection from back reflection. The two wavelength division multiplexers (WDM-1 and WDM-2) were then placed after each isolator. The 1550 nm ports of WDM-1 and WDM-2 were connected with isolators and the 2000 nm ports were connected to the gain medium. The 1.5 m long thulium-holmium doped fiber (THDF; CorActive TH-512) was used in the cavity as a gain medium. The THDF had an absorption coefficient of 15 dBm^{-1} at 1550 nm and a numerical aperture of 0.16. The length of THDF used in the setup was 1.5 m to allow suitable absorption and continuous wave (CW) laser emission at 2 μm wavelength. If a shorter THDF is used, there is a possibility of having excess pumping, and when the THDF is longer it can result in the remaining length at the end not having the required population inversion. This will not provide the required amplification and the output signal power can be low due to the re-absorption. After the THDF, the 2000 nm isolator was connected between WDM-2 and optical coupler (OC) to maintain the signal in one direction. The OC has a 90:10 output ratio, where 90% of the signal was connected to oscillate inside the cavity and 10% of the output was connected to various measuring devices to measure the lasing characteristics. The 90% port was then connected to a polarization controller (PC), and the SA was connected between the PC and the OC. Likewise, the output of the PC was then connected back with WDM-1 to complete the optical cavity.

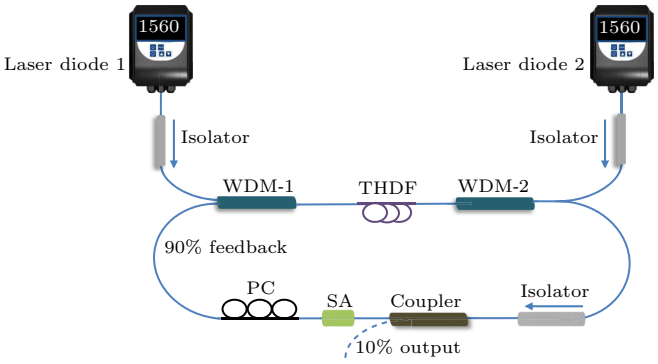


Fig. 7. Experimental setup of THDFL cavity.

The total cavity length was around 16.5 m, with a 1.5 m THDF and a 15 m single-mode fiber (SMF-28). The dispersion parameters for the SMF-28 and THDF were obtained from the manufacturers as 31.43 ps·nm^{-1}·km^{-1} and 29.1 ps·nm^{-1}·km^{-1}, at 1897 nm. The group velocity dispersion (GVD) was calculated using

$$\text{GVD} = -\frac{D(\lambda)\cdot\lambda^2}{2\cdot\pi\cdot c}, \tag{2}$$

where c is the speed of light, λ is the operating wavelength and $D(\lambda)$ is the dispersion parameter. From Eq. (2), the GVD was calculated as -0.056 ps^2·m^{-1} for the THDF and -0.060 ps^2·m^{-1} for SMF-28. Hence, the net cavity dispersion was calculated to be -0.984 ps^2 for the 16.5 m cavity length by summing up the length and GVD of the SMF and THDF.

The two antimonene-based SAs were used inside the cavity separately to generate soliton mode-locked and Q-switched pulses. For mode-locked pulses, the antimonene was coated over the tapered fiber and connected directly to the cavity. For the Q-switched laser the antimonene thin film was prepared and sandwiched between two fiber ferrules to be used as a SA. The PC was excluded from the THDFL cavity during the generation of Q-switched pulses since the polarization played a negligible role and the insertion of the PC would introduce some unwanted loss.[9,82] The various items of equipment used

for measurement of the laser output comprised a 500 MHz oscilloscope (Yokogawa DLM2054), a 1200 nm–2400 nm wavelength range OSA (Yokogawa AQ6375), a radio-frequency spectrum analyzer (RFSA; Anritsu MS2683A) an optical power meter (Thorlabs S148C) and an autocorrelator (APE PulseCheck150). Both the RFSA and oscilloscope were connected via a 2 μm InGaAs fast photodetector (Newport 818-BB-51) for optical to electrical conversion at the output.

4. Experimental results and discussion

The THDFL cavity produced a stable CW laser at a threshold pump power of 94 mW. The soliton mode-locked laser was generated when the antimonene-coated tapered fiber was incorporated in the THDFL and the power was increased to 267 mW. Figure 8 shows the mode-locked laser characteristics operated from a pump power of 267 mW–511 mW. Figure 8(a) shows the optical spectrum of the soliton mode-locked laser which operated at a central wavelength of 1897.4 nm, having a 3 dB bandwidth of 3 nm. The symmetric first-order Kelly's sidebands appeared at 1904.1 nm and 1891.88 nm, while the second-order Kelly's sidebands appeared at 1907.11 nm and 1888.87 nm. The presence of dips in the optical spectrum is due to moisture absorption at the 2 μm wavelength region.[83] The laser operated at a repetition rate of 12.6 MHz and the pulse period was 79.3 ns, as illustrated in Fig. 8(b). Figure 8(c) represents the RF spectrum of the mode-locked laser within a 1000 MHz frequency span. The consistent frequency spectrum having more than 83 frequency harmonics showed that laser operation was stable for a longer time. The inset of Fig. 8(c) shows that the signal-to-noise ratio (SNR) of the fundamental frequency was 64 dB. Figure 8(d) represents the autocorrelator trace of the mode-locked pulse, where the blue line shows the experimental result and the red

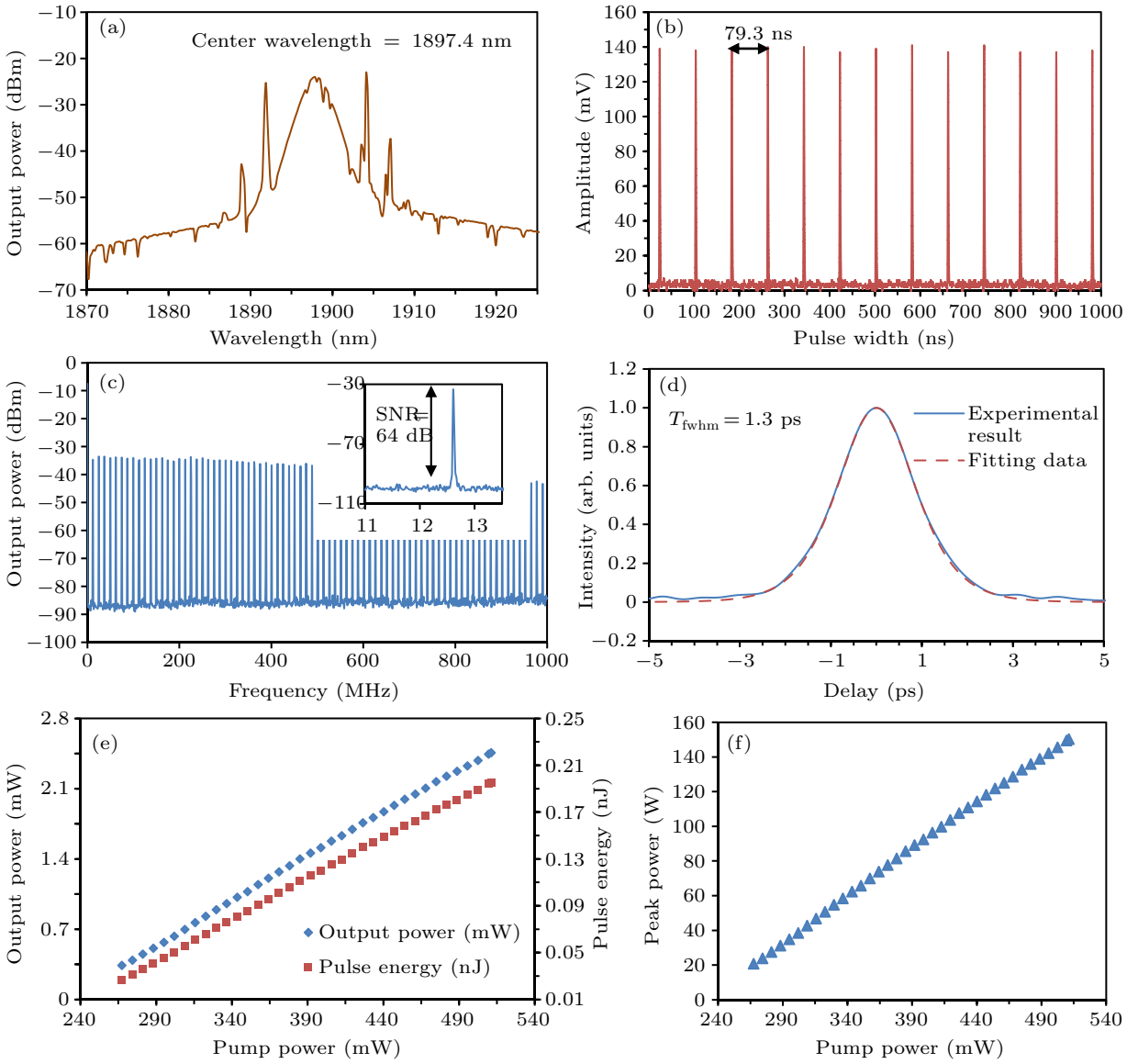


Fig. 8. Soliton mode-locked pulses: (a) optical spectrum, (b) pulse train, (c) RF spectrum, (d) autocorrelator trace, (e) output power and pulse energy against pump power and (f) peak power against pump power.

dashed lines are the fitting data from the autocorrelator. The data fitted well over the autocorrelator trace and the laser pulse width or full width at half maximum ($T_{\rm fwhm}$) was about 1.3 ps. The calculated time–bandwidth product was around 0.324, which is slightly higher than the typical value of sech^2 fitting of 0.315, indicating that the pulses were marginally chirped. The relationship of pump power with output power and pulse energy is plotted in Fig. 8(e). Within the pump power range of 267 mW–511 mW, both the output power and pulse energy increased linearly with increasing pump power. The output power increased from 0.34 mW to 2.46 mW and the highest pulse achieved was 0.2 nJ. The corresponding peak power also increased linearly with the increase in pump power, and the maximum peak power achieved was about 150 W, as plotted in Fig. 8(f).

The interplay of cavity dispersion and nonlinearity within the laser cavity helps to achieve a soliton mode-locked laser. The appearance of Kelly's sidebands in soliton mode-locked lasers is due to the periodic disturbance of solitons as they experience loss and gain during propagation in the resonating laser cavity.[84] A further increase in the length of the tapered fiber and also the different concentrations of antimonene may also result in a higher modulation depth, which may reduce the pulse width.[85] Thus, the pulse width can also be reduced further by shortening the cavity length.

Since the mode-locking pulses were stable up to the maximum operating pump power of 511 mW there is no visible damage to the SA. Thus, mode-locked pulses could be repeated by increasing and decreasing the pump power. The optical damage threshold for the SA can be estimated by measuring the average output power, which is 2.46 mW at the 10% output coupler. Therefore, the average oscillating power in the cavity was 24.6 mW. By taking the repetition rate and the pulse width values of 12.6 MHz and 1.3 ps, the pulse energy can be calculated by dividing the maximum average output power by the repetition rate. The peak power can be calculated by dividing the pulse energy by the pulse width. The corresponding pulse energy and peak power in the cavity were 1.95 nJ and 1.5 kW. Since the cavity mostly comprises optical components with SMF-28 fiber having a core diameter of 9 μm, the corresponding peak power intensity would be 2.36 GW·cm^{-2}. Stable mode-locked pulses were obtained even at this maximum pump power of 511 mW; this indicates that the damage threshold of this SA is higher than 2.36 GW·cm^{-2}.

Figure 9 shows the long-term stability of the mode-locked laser achieved by using an antimonene-based SA. The optical spectrum of the mode-locked laser was recorded for 3 h at intervals of 30 min, as shown in Fig. 9(a). Under normal laboratory conditions, a stable mode-locked laser was observed for 3 h with no significant shift in the central wavelength. The stability of the central wavelength and its power intensity against time is plotted in Fig. 9(b). The wavelength spectrum remains stable around 1897.4 nm with a negligible shift of about 0.2 nm, while the output power at the central wavelength is also stable with a marginal change of ±0.1 dB. This indicates that the SA could sustain long-term illumination without being damaged.

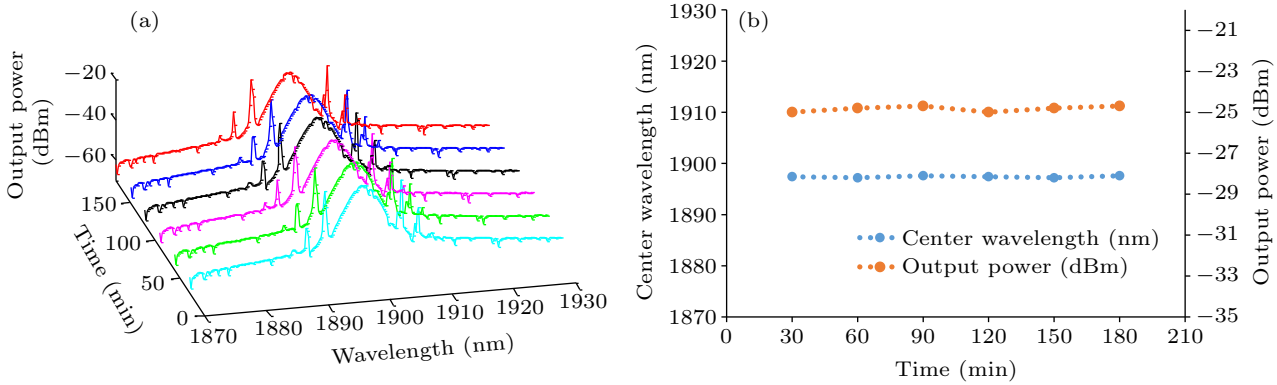


Fig. 9. Stability of the mode-locked laser using an antimonene SA: (a) optical spectrum for 3 h, taken at every 30 min, and (b) central wavelength and output power for 3 h.

A self-started Q-switched laser was achieved when the antimonene thin film was inserted into the THDFL cavity and the pump power was increased to 312 mW. Figure 10 represents the Q-switched THDFL characteristics achieved by using an antimonene SA. The Q-switched laser operated at a central wavelength of 1890.1 nm, and the optical spectrum of the Q-switched laser at 381 mW pump power is shown in Fig. 10(a). The pulse trains at pump powers of 312 mW and 381 mW are given in Figs. 10(b) and 10(c).

At a pump power of 312 mW, the repetition rate and pulse width were 36 kHz and 3.85 μs, respectively. When the pump power was increased to 381 mW, the repetition rate increased to the maximum of 56.63 kHz and the pulse width gradually decreased to 2.85 μs, represented as insets to Figs. 10(b) and 10(c), respectively. In Fig. 10(d), the repetition rate was recorded within the 1400 kHz frequency span at

a pump power of 381 mW. As shown in the inset of Fig. 10(d), the fundamental frequency was 56.63 kHz and the SNR of the fundamental frequency was 54.6 dB. The change in repetition rate and pulse width against pump power is plotted in Fig. 10(e). The *Q*-switched laser was stable from 312 mW to 381 mW and the repetition rate increased with increase in pump power, while the pulse width decreased with increase in pump power. This behavior of increase in repetition rate and decrease in pulse width against increase in pump power justified the typical characteristics of a *Q*-switched laser.[86,87] The *Q*-switched laser pulse width can be further shortened by optimizing both the cavity length and preparation of the SA. Several antimonene-based SAs can be prepared at different concentrations and thicknesses to optimize SA preparation, which may lead to further reduction of the *Q*-switched pulse width.[88,89] A shorter cavity length can also reduce the pulse width; however, a shorter THDF may have a lower gain, resulting in lower output power. The trend of increase in output power and pulse energy with respect to pump power is presented in Fig. 10(f). The output power first gradually increases from 0.014 mW to 0.024 mW and then increases almost linearly to the maximum of 0.484 mW. The corresponding pulse energy also increases with the increase in pump power, to the maximum of 8.54 nJ at a pump power of 381 mW.

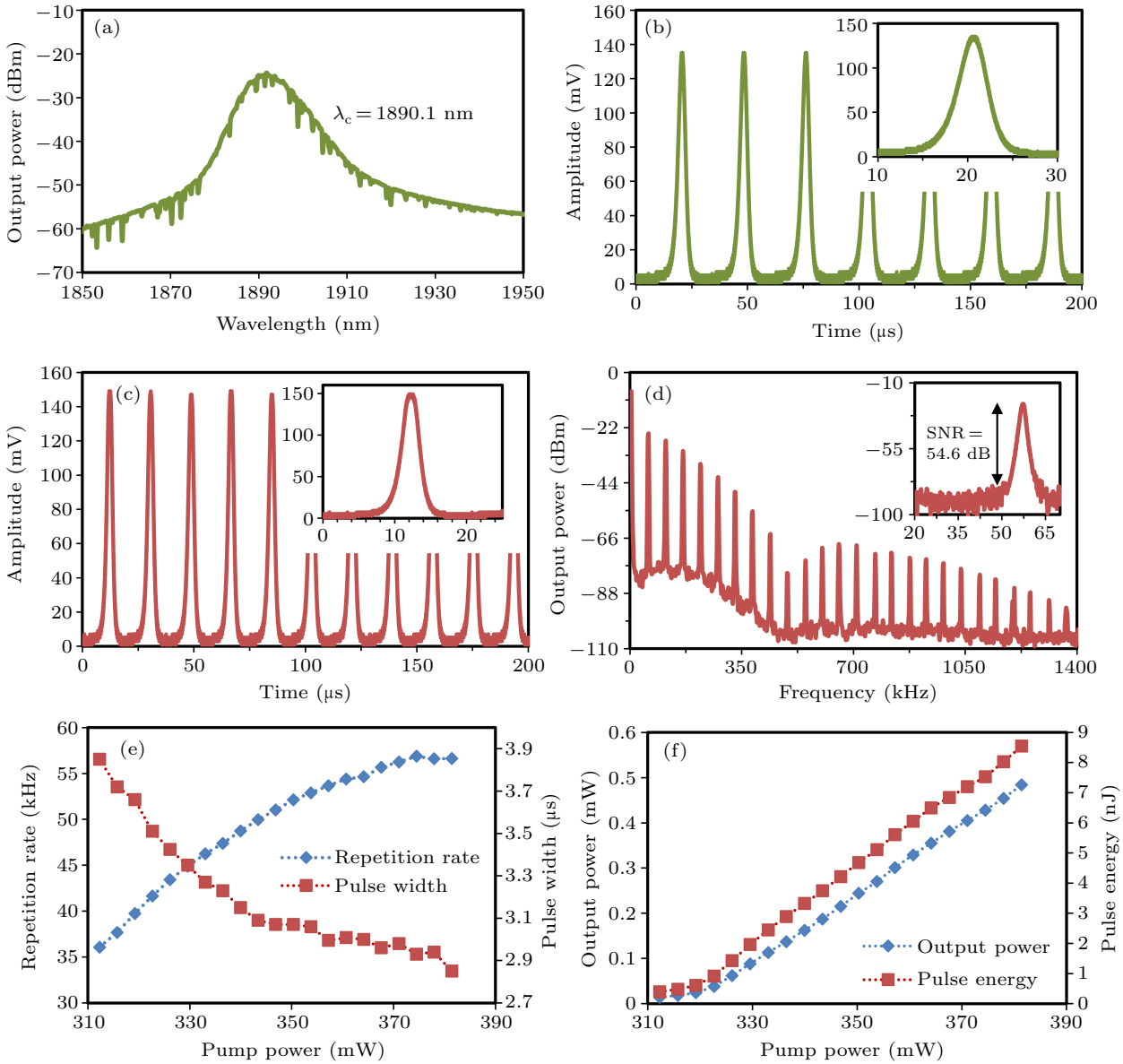


Fig. 10. The *Q*-switched laser using an antimonene SA: (a) optical spectrum at 381 mW pump power, (b) pulse train at 312 mW pump power, (c) pulse train at 381 mW pump power, (d) RF spectrum at 381 mW pump power, (e) variation of repetition rate and pulse width with pump power and (f) output power and pulse energy against pump power.

The TBF was added to the cavity between the antimonene thin-film SA and the 90/10 coupler to filter out the wavelength and achieve bandwidth tunability of the *Q*-switched laser output. The pump power was increased to 511 mW to compensate for TBF insertion loss and to stabilize the *Q*-switched pulses and output power. As demonstrated in Fig. 11(a),

the *Q*-switched laser was widely tunable within a range of 54 nm spanning from 1882 nm to 1936 nm at a spacing interval of 6 nm. After taking about ten scans, the intensity peak remained almost unchanged for wavelength tuning from 1882 nm to 1936 nm, indicating that tunable *Q*-switched laser operation was stable. This wavelength tunable *Q*-switched laser can be applied as a source for several applications, such as in dense wavelength division multiplexing for optical communication, spectroscopy, sensing, biomedical applications and LIDAR sensing.[90] The laser was tunable around a wavelength of 2 μm as demonstrated in the present work using THDF as the gain medium, which has an emission spectrum of 2 μm. There have also been reports on using antimonene to operate at different wavelengths, such as in 1.5 μm as demonstrated in Refs. [74,91] using erbium-doped fiber as the gain medium. This shows the ability to use antimonene as a SA over a wider wavelength range. Figure 11(b) shows the trend of repetition rate and pulse width within the same wavelength tunability range of 1882 nm–1936 nm. The pulse width varied slightly between 3 μs and 3.1 μs and the repetition rate followed the ASE gain spectrum (inset Fig. 11(b)).

Table 1 compares the results of the present work with other reports using antimony-based SAs to generate *Q*-switched and mode-locked lasers at 1.5 μm and 2 μm wavelengths.

The incorporation of an antimony SA produced the shortest pulse width of 3.53 ps for the mode-locked EDFL[71] and 5.36 μs for the *Q*-switched laser.[92] Rahman *et al*. reported *Q*-switched and mode-locked lasers by using antimony-based SAs at a 2 μm wavelength which could produce the shortest pulse width of about 4.9 μs and 64 ps, respectively.[73] Furthermore, antimonene-based SAs are rarely explored, and the incorporation of an antimonene SA is only reported for the 1.5 μm wavelength region.[74,75] Although Yuan *et al*. have reported a *Q*-switched laser using an antimonene SA, the laser operated at the shorter wavelength of 1558 nm.[74] In this work, we have reported the generation of both *Q*-switched and mode-locked laser pulses obtained by incorporating an antimonene SA in the eye-safe region of 2 μm wavelength. Our work reports a shorter pulse width of 1.3 ps by using an antimonene SA in the 2 μm wavelength region compared with a 64 ps pulse mode-locked laser achieved with an antimony SA.[73]

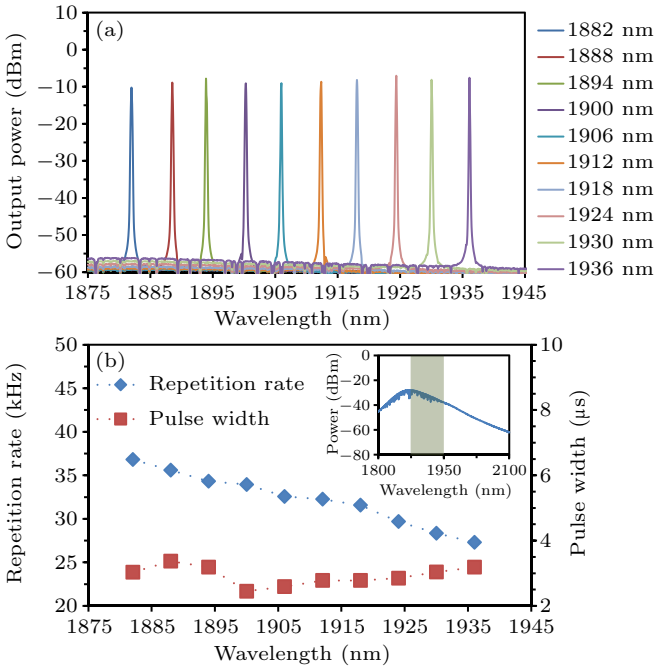


Fig. 11. Tunable *Q*-switched operation: (a) wavelength tunability between 1882 nm and 1936 nm and (b) repetition rate and pulse width of the tunable *Q*-switched laser.

Table 1. Comparison of the results of our work with *Q*-switched and mode-locked lasers produced by antimony and antimonene-based SAs at different wavelengths.

SA	Laser operation	Central wavelength (nm)	Lasing medium	Repetition rate	SNR (dB)	Pulse width	Output power (mW)	Pulse energy (nJ)	Ref.
Antimony	mode-locked	1559	EDFL	0.99 MHz	70	3.53 ps	20.43	20.59	[71]
Antimony	*Q*-switched	1559	EDFL	70.82 kHz–98.04 kHz	74	7.42 μs–5.36 μs	8.45	86.19	[92]
Antimony	mode-locked	1914	TDFL	8.65 MHz	77	64 ps	6.5	0.75	[73]
Antimony	*Q*-switched	1947	TDFL	14.5 kHz–23.5 kHz	47	11.6 μs–4.9 μs	1.3–2.8	79.21–120.12	[73]
Antimonene	*Q*-switched	1558	EDFL	25.6 kHz–124.1 kHz	48	5.1 μs–1.42 μs	4.73	54	[74]
Antimonene	mode-locked	1897.4	THDFL	12.6 MHz	64	1.3 ps	2.46	0.2	this work
Antimonene	*Q*-switched	1890.1	THDFL	36 kHz–56.63 kHz	54.6	3.85 μs–2.85 μs	0.484	8.54	this work

5. Conclusion

Few-layers antimonene was prepared and successfully used as a SA to generate mode-locked and tunable *Q*-switched lasers in the 2 μm region. A soliton mode-locked laser was obtained by depositing antimonene onto a tapered fiber that was then inserted into a THDFL cavity. The soliton mode-locked laser had a central wavelength of 1890.1 nm and a pulse width of 1.3 ps. The maximum output power and the pulse energy of the mode-locked THDFL were 2.46 mW and 0.2 nJ, respectively. For tunable *Q*-switching operation, few-layer antimonene was prepared in thin film form and placed between two fiber ferrules that were fixed using a FC/PC connector. The *Q*-switched pulse had pulse widths varying from 3.85 μs to 2.85 μs with repetition rates ranging from 36 kHz

to 56.63 kHz. Wide wavelength tunability was also observed for the *Q*-switched laser, ranging from 1882 nm to 1936 nm by using a TBF. The results show that few-layers antimonene was suitable for use as a SA to successfully generate mode-locked and *Q*-switched pulses in the 2 μm region, and these lasers could be useful for medical applications.

Acknowledgments

We would like to thank the Ministry of Higher Education, Malaysia for their support for this work through Grant, HiCoE (PRC-2022) and the Universiti Malaya for the funding of this work through Grant Nos. RU005-2021 and MGO23-2022.

References

[1] Correa D S, Cardoso M R, Tribuzi V, Misoguti L and Mendonca C R 2011 *IEEE J. Sel. Top. Quant.* **18** 176
[2] Tanzi E and Alster T 2004 *Skin Therapy Lett.* **9** 4
[3] Shoji T, Kuroda H, Suzuki M, Ibuki H, Araie M and Yoneya S 2017 *Plos One* **12** e0181675
[4] Spiers G D, Menzies R T, Jacob J, Christensen L E, Phillips M W, Choi Y and Browell E V 2011 *Appl. Opt.* **50** 2098
[5] Van Den Eeckhaut M, Kerle N, Poesen J and Hervás J 2012 *Geomorphology* **173–174** 30
[6] O'Mahony M J, Simeonidou D, Hunter D K and Tzanakaki A 2001 *IEEE Commun. Mag.* **39** 128
[7] Sugar A 2002 *Current Opinion in Ophthalmology* **13** 246
[8] Salam S, Nizamani B, Azooz S M, Fizza G, Yasin M and Harun S W 2021 *Appl. Opt.* **60** 3149
[9] Nizamani B, Jafry A, Salam S, Najm M M, Khudus M A, Hanafi E and Harun S 2020 *Opt. Commun.* **475** 126217
[10] Nizamani B, Jafry A, Salam S, Fizza G, Soboh R, Khudus M A, Hanafi E, Yasin M and Harun S 2021 *Laser Physics* **31** 055101
[11] Muhammad A R, Zakaria R, Ahmad M T, Wang P and Harun S W 2019 *Optical Fiber Technology* **50** 23
[12] Rusdi M F M, Latiff A A, Paul M C, Das S, Dhar A, Ahmad H and Harun S W 2017 *Opt. Laser Technol.* **89** 16
[13] Scholle K, Lamrini S, Koopmann P and Fuhrberg P 2010 *Frontiers in Guided Wave Optics and Optoelectronics* (IntechOpen)
[14] Singh U N, Yu J, Petros M, Refaat T and Reithmaier K 2014 *Lidar Remote Sensing for Environmental Monitoring XIV*, p. 887209
[15] Pal A, Chen S Y, Sen R, Sun T and Grattan K 2013 *Laser Phys. Lett.* **10** 085101
[16] Cuadrado-Laborde C, DíEz A, Cruz J and Andrés M 2010 *Appl. Phys. B* **99** 95
[17] Chen H, Chen S P, Jiang Z F and Hou J 2015 *Opt. Express* **23** 1308
[18] Keller U, Weingarten K J, Kartner F X, Kopf D, Braun B, Jung I D, Fluck R, Honninger C, Matuschek N and Der Au J A 1996 *IEEE Journal of Selected Topics in Quantum Electronics* **2** 435
[19] Jafry A, Kasim N, Rusdi M, Rosol A, Yusoff R, Muhammad A, Nizamani B and Harun S 2020 *Opt. Laser Technol.* **127** 106186
[20] Miao R, Tong M, Yin K, Ouyang H, Wang Z, Zheng X and Jiang T 2019 *Chin. Opt. Lett.* **17** 071403
[21] Gong Q and Zhao W 2021 *Ultrafast Sci.* **2021** 9765859
[22] Salam S, Harun S W, Al-Masoodi A H, Ahmed M H, Al-Masoodi A H, Alani I A, Majid W H A, Wong W R and Yasin M 2019 *Iet Optoelectron.* **13** 247
[23] Najm M M, Arof H, Nizamani B, Al-Hiti A S, Zhang P, Yasin M and Harun S W 2021 *J. Modern Opt.* **68** 237
[24] Rahman M F A, Rusdi M F M, Lokman M Q, Mahyuddin M B H, Latiff A A, Rosol A H A, Dimyati K and Harun S W 2017 *Chin. Phys. Lett.* **34** 054201
[25] Rosol A H A, Mahyuddin M, Musa N, Aziz M, Khudus M I M A, Yasin M and Harun S W 2021 *Optik* **227** 165976
[26] Nizamani B, Khudus M A, Salam S, Najm M M, Jafry A, Hanafi E, Yasin M and Harun S W 2021 *Res. Opt.* **3** 100057
[27] Ahmad M T, Rusdi M F M, Jafry A, Latiff A A, Zakaria R, Zainuddin N A a M, Arof H, Ahmad H and Harun S W 2019 *Opt. Fiber Technol.* **53** 101997
[28] Nizamani B, Salam S, Jafry A, Zahir N, Jurami N, Khudus M A, Shuhaimi A, Hanafi E and Harun S 2020 *Chin. Phys. Lett.* **37** 054202
[29] Ismail M A, Harun S W, Zulkepely N R, Nor R M, Ahmad F and Ahmad H 2012 *Appl. Opt.* **51** 8621
[30] Lau K Y, Ker P J, Abas A F, Alresheedi M T and Mahdi M A 2019 *Chin. Opt. Lett.* **17** 051401
[31] Fu B, Hua Y, Xiao X, Zhu H, Sun Z and Yang C 2014 *IEEE J. Sel. Top. Quant.* **20** 411
[32] Zhao L, Tang D, Zhang H, Wu X, Bao Q and Loh K P 2010 *Opt. Lett.* **35** 3622
[33] Sun Z, Hasan T, Torrisi F, Popa D, Privitera G, Wang F, Bonaccorso F, Basko D M and Ferrari A C 2010 *ACS Nano* **4** 803
[34] Luo Z, Zhou M, Weng J, Huang G, Xu H, Ye C and Cai Z 2010 *Opt. Lett.* **35** 3709
[35] Sotor J, Sobon G, Macherzynski W, Paletko P and Abramski K M 2015 *Appl. Phys. Lett.* **107** 051108
[36] Mayorga-Martinez C C, Sofer Z and Pumera M 2015 *Angewandte Chemie International Edition* **54** 14317
[37] Island J O, Steele G A, van der Zant H S and Castellanos-Gomez A 2015 *2D Mater* **2** 011002
[38] Guo B, Xiao Q l, Wang S H and Zhang H 2019 *Laser Photon. Rev.* **13** 1800327
[39] Liu X, Guo Q and Qiu J 2017 *Adv. Mater* **29** 1605886
[40] Wu Q, Jin X, Chen S, Jiang X, Hu Y, Jiang Q, Wu L, Li J, Zheng Z and Zhang M 2019 *Opt. Express* **27** 10159
[41] Najm M M, Al-Hiti A S, Nizamani B, Zhang P, Arof H, Rosol A H A, Yasin M and Harun S W 2021 *Opt. Eng.* **60** 066116
[42] Jafry A A A, Kasim N, Nizamani B, Muhammad A R, Harun S W and Yupapin P 2020 *Optik* **224** 165682
[43] Rosol A H A, Jafry A A A, Nizamani B, Zulkipli N F, Khudus M I M A, Yasin M and Harun S W 2021 *J. Modern Opt.* **68** 984
[44] Ahmad H, Ismail N, Aidit S, Reduan S, Samion M and Yusoff N 2021 *Opt. Commun.* **490** 126888
[45] Wang C, Peng Q Q, Fan X W, Liang W Y, Zhang F, Liu J and Zhang H 2018 *Chin. Phys. B* **27** 094214
[46] Khazaeinezhad R, Kassani S H, Jeong H, Nazari T, Yeom D I and Oh K 2014 *IEEE Photon. J.* **7** 1
[47] Ahmad H, Hassan H, Safaei R, Thambiratnam K, Ismail M and Amiri I 2017 *Opt. Commun.* **400** 55
[48] Li L, Su Y, Wang Y, Wang X, Wang Y, Li X, Mao D and Si J 2016 *IEEE J. Sel. Top. Quant.* **23** 44
[49] Najm M M, Harun S W, Salam S, Arof H, Nizamani B and Yasin M 2021 *Opt. Fiber Technol.* **61** 102439
[50] Nizamani B, Jafry A, Khudus M A, Rosol A, Samsamnun F, Kasim N, Hanafi E, Shuhaimi A and Harun S 2020 *Opt. Fiber Technol.* **55** 102124
[51] Ahmad H, Ismail M A, Sathiyan S, Reduan S A, Ruslan N, Lee C S J, Zulkifli M Z, Thambiratnam K, Ismail M F and Harun S W 2017 *Opt. Commun.* **382** 93
[52] Liu M L, OuYang Y Y, Hou H R, Lei M, Liu W J and Wei Z Y 2018 *Chin. Phys. B* **27** 084211
[53] Rosdin R Z R R, Ahmad M T, Muhammad A R, Jusoh Z, Arof H and Harun S W 2019 *Chin. Phys. Lett.* **36** 054202
[54] Li L, Pang L, Wang R, Zhang X, Hui Z, Han D, Zhao F and Liu W 2022 *Laser Photon. Rev.* **16** 2100255
[55] Pang L, Sun Z, Zhao Q, Wang R, Yuan L, Wu R, Lv Y and Liu W 2021 *ACS Appl. Mater. Interfaces* **13** 28721
[56] Li L, Pang L, Wang Y and Liu W 2021 *Nanoscale* **13** 2511
[57] Liu W, Shi T, Liu M, Wang Q, Liu X, Zhou Q, Lei M, Lu P, Yu L and Wei Z 2021 *Opt. Express* **29** 29402
[58] Ares P, Zamora F and Gomez-Herrero J 2017 *ACS Photon.* **4** 600
[59] AktüRk O Ü, ÖZçlik V O and Ciraci S 2015 *Phys. Rev. B* **91** 235446
[60] Zhang L, Fahad S, Wu H R, Dong T T, Chen Z Z, Zhang Z Q, Liu R T, Zhai X P, Li X Y and Fei X 2020 *Nanoscale Horizons* **5** 1420
[61] Singh D, Gupta S K, Sonvane Y and Lukačević I 2016 *J. Mater. Chem. C* **4** 6386
[62] MartíNez-Periñán E, Down M P, Gibaja C, Lorenzo E, Zamora F and Banks C E 2018 *Adv. Energy Mater.* **8** 1702606
[63] Zhang C, Li Y, Zhang P, Qiu M, Jiang X and Zhang H 2019 *Sol. Energy Mat. Sol. C* **189** 11
[64] Wang G, Pandey R and Karna S P 2015 *ACS Appl. Mater. Inter.* **7** 11490

[65] Zhang S, Yan Z, Li Y, Chen Z and Zeng H 2015 *Angewandte Chemie* **127** 3155

[66] Zhang F, Jiang X, He Z, Liang W, Xu S and Zhang H 2019 *Opt. Mater.* **95** 109209

[67] Ares P, Aguilar-Galindo F, Rodríguez-San-Miguel D, Aldave D A, Díaz-Tendero S, Alcamí M, Martín F, Gómez-Herrero J and Zamora F 2016 *Adv. Mater.* **28** 6332

[68] Zhang F, Wu Z, Wang Z, Wang D, Wang S and Xu X 2016 *RSC Adv.* **6** 20027

[69] Wu J, Wei Y, Shen W, Xiong Y, Lin C, Gao Y, AL-Ammari A, Liu K, Ma T and Chen J 2020 *Appl. Phys. Lett.* **116** 261903

[70] Lu L, Tang X, Cao R, Wu L, Li Z, Jing G, Dong B, Lu S, Li Y and Xiang Y 2017 *Adv. Opt. Mater.* **5** 1700301

[71] Ab Rahman M F, Latiff A A, Rosol A H A, Dimyati K, Wang P and Harun S W 2018 *J. Lightwave Technol.* **36** 3522

[72] Du L, Lu D, Li J, Yang L, Yang K, Huang B, Miao L, Qi X, Zhao C and Zhong J 2020 *IEEE J. Sel. Top. Quant.* **27** 1

[73] Rahman M F A, Latiff A A, Zaidi U Z M, Rusdi M F M, Rosol A H A, Bushroa A R, Dimyati K and Harun S W 2018 *Opt. Commun.* **421** 99

[74] Yuan J, Liu G, Xin Y, Xing F, Han K, Zhang W, Zhang F and Fu S 2021 *Opt. Mater.* **118** 111256

[75] Hu P, Liu Y, Guo L, Ge X, Liu X, Yu L and Liu Q 2019 *Appl. Opt.* **58** 7845

[76] Gao Y, Tian W, Huo C, Zhang K, Guo S, Zhang S, Song X, Jiang L, Huo K and Zeng H 2019 *J. Mater. Chem. A* **7** 3238

[77] Ismail M M, Vigneshwaran J, Arunbalaji S, Mani D, Arivanandhan M, Jose S P and Jayavel R 2020 *Dalton Trans.* **49** 13717

[78] Ahmad H, Ramli R, Samion M Z and Yusoff N 2021 *Optik* **245** 167723

[79] Du J, Wang Q, Jiang G, Xu C, Zhao C, Xiang Y, Chen Y, Wen S and Zhang H 2014 *Sci. Rep.* **4** 1

[80] Zhang R L, Wang J, Liao M S, Li X, Guan P W, Liu Y Y, Zhou Y and Gao W Q 2019 *Chin. Phys. B* **28** 034203

[81] Ahmad H, Azri M, Ramli R, Samion M, Yusoff N and Lim K 2021 *Sci. Rep.* **11** 21278

[82] Najm M M, Al-Hiti A S, Nizamani B, Arof H, Zhang P, Yasin M and Harun S W 2021 *Optik* **242** 167073

[83] Sotor J, Sobon G, Kowalczyk M, Macherzynski W, Paletko P and Abramski K M 2015 *Opt. Lett.* **40** 3885

[84] Wang Y, Fu S, Zhang C, Tang X, Kong J, Lee J H and Zhao L 2021 *J. Lightwave Technol.* **39** 2542

[85] Jafry A A A, Rosol A H A, Kasim N, Muhammad A R, Rulaningtyas R, Yasin M and Harun S W 2020 *Appl. Opt.* **59** 8759

[86] Nizamani B, Jafry A, Khudus M A, Memon F, Shuhaimi A, Kasim N, Hanafi E, Yasin M and Harun S 2020 *Opt. Laser Technol.* **124** 105998

[87] Degnan J J 1995 *IEEE J. Quant. Electron.* **31** 1890

[88] Najm M M, Al-Hiti A S, Nizamani B, Abdullah M N, Rosol A, Zhang P, Najm S M, Arof H, Tiu Z C and Yasin M 2022 *Opt. Fiber Technol.* **70** 102853

[89] Li D, Jussila H, Karvonen L, Ye G, Lipsanen H, Chen X and Sun Z 2015 *Sci. Rep.* **5** 1

[90] Sharma U, Kim C S and Kang J U 2004 *IEEE Photon. Technol. Lett.* **16** 1277

[91] Liu G, Zhang F, Wu T, Li Z, Zhang W, Han K, Xing F, Man Z, Ge X and Fu S 2019 *IEEE Photon. J.* **11** 1

[92] Rahman M, Zhalilah M, Latiff A, Rosol A, Lokman M, Bushroa A R, Dimyati K and Harun S W 2018 *J. Modern Opt.* **65** 811